Chemical Science

ROYAL SOCIETY OF CHEMISTRY

EDGE ARTICLE

View Article Online
View Journal

Cite this: DOI: 10.1039/d4sc04968c

All publication charges for this article have been paid for by the Royal Society of Chemistry

Chiroptical properties of cyanine aggregates: hierarchical modelling from monomers to bundles†

Francesco Bertocchi,‡[a] Shahana Nizar, ‡[b] Cristina Sissa, [a] Minghao Li, [c] Thomas W. Ebbesen,[b] Cyriaque Genet*[b] and Anna Painelli *[a]

Some achiral cyanine dyes form well-ordered chiral assemblies exhibiting pronounced Circular Dichroism (CD) and Circularly Polarized Luminescence (CPL). Notably, achiral C8O3 cyanines self-assemble into tubular J-aggregates, which further organize into bundles displaying bisignate CD spectrum – hallmark of an exciton coupled system – and an unusual bisignated CPL. In contrast, the tubular aggregates display a monosignate CD spectrum. The mechanism underlying these intriguing features remains elusive. In the present work, a quantum-mechanical exciton model is proposed to elucidate the (chir) optical behaviour of C8O3 aggregates. A herringbone arrangement of C8O3 dyes within the tubular aggregates well reproduces the observed spectral signatures. The anomalous observation of a singular CD peak in tubular aggregates is ascribed to the intrinsic chirality of the monomeric units inside the aggregate, whereas the CD doublet characterizing the bundles is attributed to the exciton coupling between the constituent tubes. The bisignated CPL signal observed in bundles reveals significant anti-Kasha emission at room temperature and is quantitatively addressed accounting for a very tiny exciton splitting leading to a sizable thermal population of both exciton states. This study provides crucial insights on the complexity of C8O3 aggregation and on the origin of chiroptical response at various aggregation stages.

Received 25th July 2024
Accepted 8th September 2024

DOI: 10.1039/d4sc04968c

rsc.li/chemical-science

1 Introduction

Chiral molecules, having structures not superimposable with their mirror image,[1–3] play a crucial role in various biological, chemical, and physical phenomena.[4–8] Circular dichroism (CD), measuring the differential absorption of left-handed and right-handed circularly polarized light,[9,10] is the spectroscopic technique of choice to investigate chiral structures. Circularly Polarized Luminescence (CPL), the analogous phenomenon of CD but detected in emission,[11,12] has garnered considerable attention in recent years for its potential technological applications in CP-OLED devices,[13–15] 3D-displays and anti-counterfeiting inks.[16] Successful applications require large dissymmetry factors, defined in absorption as $g_{abs} = 2(A_L - A_R)/(A_L + A_R)$, where $A_{L(R)}$ is the sample absorbance of left(right)-handed circularly polarized light and in emission as $g_{lum} = 2(I_L - I_R)/(I_L + I_R)$, where $I_{L(R)}$ is the intensity of the emitted left(right)-handed circularly polarized light. Enhancing the dissymmetry factors is the focus of intense current research.[14,17–20] In this context, supramolecular aggregation is emerging as a promising strategy to improve chiroptical properties, primarily through an exciton coupling mechanism.[21–26]

Cyanines are a large family of dyes with remarkable aggregation behavior.[27–31] Among them, 3,3′-bis(2-sulfopropyl)-5,5′,6,6′-tetrachloro-1,1′-dioctylbenzimidacarbocyanine (C8S3) and 3,3′-bis(3-carboxy-*n*-propyl)-3,3′-di-*n*-octyl-5,5′,6,6′-tetrachlorobenzimidacarbocyanine (C8O3) cyanines show an impressive propensity to form strongly coupled supramolecular aggregates in polar environments and in thin films.[32–35] In 1996, the spontaneous aggregation of C8O3 molecules into non-racemic chiral aggregates was observed, an astonishing result since the chromophoric core of the monomer, in its equilibrium geometry, is planar and nonchiral.[36] The aggregation of C8O3 is hierarchical, with different structural features appearing in successive size scales:[37] monomers assemble into J-aggregates in the shapes of tubes, which in turn interweave to form bundles,[38–40] as schematically shown in the top panels of Fig. 1. In each aggregation step, notable spectroscopic features appear, ascribed to a strong exciton coupling among the constituent units. Previous studies from some of us revealed robust chiroptical responses through hierarchical aggregation of C8O3 in solution,[41] and a perfectly correlated g_{abs} and g_{lum}, for C8O3 bundles in films reaching an impressive g_{lum} of 0.08.[42]

[a]Dipartimento di Scienze Chimiche, della Vita e della Sostenibilità Ambientale, Università di Parma, Parco Area delle Scienze 17A, Parma, 43124, Italy. E-mail: anna.painelli@unipr.it

[b]CNRS, CESQ-ISIS University of Strasbourg (UMR 7006), F-67000 Strasbourg, France. E-mail: genet@unistra.fr

[c]Quantum Sensing Laboratory, Department of Physics, University of Basel, Switzerland

† Electronic supplementary information (ESI) available. See DOI: https://doi.org/10.1039/d4sc04968c

‡ Equally contributing authors.

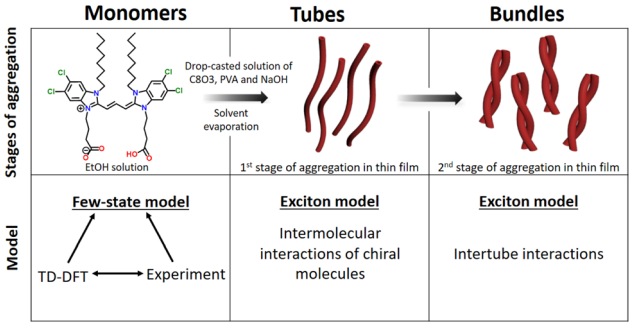

Fig. 1 Upper panels: various stages of aggregation and relevant experimental conditions. Lower panels: theoretical models employed to describe each stage of aggregation.

Moreover, several uncommon chiroptical features were uncovered. Specifically, individual C8O3 tubes displayed a single CD peak instead of the typical doublet indicative of exciton coupling,[9,23,25] leading to an apparent violation of the "sum rule". This rule, first enunciated by Condon,[43] states that the integrated area beneath a CD spectrum vanishes. Adding complexity to the problem, a CD doublet pattern appears for bundled aggregates, which also show a remarkable bisignate CPL, indicative of uncommon double emission at room temperature and anti-Kasha behaviour. Given their importance, these features need to be analyzed and understood.

Here we clarify the distinctive spectral characteristics exhibited by C8O3 aggregates and rationalize the chiroptical features present at each tier of the hierarchical structure in C8O3 aggregates. A bottom-up modeling approach is adopted,[44–46] as illustrated in the bottom panels of Fig. 1. A joint analysis of experimental data for the monomer in solution and TD-DFT computational results lead to a reliable description and parametrization of a model for the C8O3 monomer. This approach sets a sound basis to construct a model for the aggregates in the tubular form and then to describe the bundles as hierarchical assemblies of tubes. The multiscale theoretical protocol proposed in this work enables the investigation of the complex aggregation phenomena observed in C8O3 at different aggregation stages. The unusual spectral features observed in experimental spectra are addressed, providing a complete picture of their physical origin.

2 Results and discussion

In Section 2.1 we shortly summarize relevant experimental data, addressing the evolution of chiroptical spectra of C8O3 when going from solution to tubular aggregates and finally bundles.[42] The theoretical analysis begins in Section 2.2 where a minimal model for the C8O3 dye is proposed and parametrized, relying on TD-DFT calculations on the distorted chromophoric core, as extracted from the crystal structure. The dyes are then assembled to form a tubular aggregate (Section 2.3) whose spectral properties are analyzed relying on an exciton model for intermolecular electrostatic interactions. Finally, in Section 2.4 a model is proposed for the bundle that quantitatively accounts for CD spectra and even more interestingly for the observation of a bisignate CPL feature.

2.1 Experimental data analysis

Our analysis mainly relies on experimental data collected in a previous study by some of us.[41,42] The preparation of a film of C8O3 aggregates begins by mixing a monomeric C8O3 solution (0.25 mM in ethanol) with an aqueous PVA/NaOH solution at a 1 : 1 volume ratio. The PVA/NaOH solution is made by combining 6 wt% PVA and 10 mM NaOH aqueous solutions, also in a 1 : 1 volume ratio. After dropcasting the resulting C8O3/PVA/NaOH mixture onto a glass substrate, solvent evaporation triggers a hierarchical aggregation process. This process initially forms tubular structures that subsequently intertwine to create bundles (*cf.* Fig. 1). A comprehensive analysis of thin films of C8O3 aggregates exploiting Mueller polarimetry[41,47] allowed for the artefact-free acquisition of absorption, emission, Circular Dichroism (CD), and Circularly Polarized Luminescence (CPL) spectra of the aggregates. Using a microscope objective within the Mueller setup, light could be focused on specific sample regions containing either individual tubes or bundles. Fig. 2 summarizes experimental (chiro)optical spectra obtained for the monomer in solution and for single tubes and bundles in thin films.

The main absorption peak shows a large red shift when going from solution (~520 nm) to either the tubes or the bundles (~610 nm), indicative of strong J-aggregation, as further supported by the intense emission observed in the aggregates with negligible Stokes shift.[31,48,49] The narrowing of J-aggregates absorption is ascribed to the reduced electron–vibration coupling as due to exciton delocalization.[49] The absorption spectra of tubes and bundles show, besides the prominent sharp peak at 610 nm, a secondary less intense, broad peak at shorter wavelength (~575 nm). Linear dichroism measurements on oriented samples of tubular aggregates

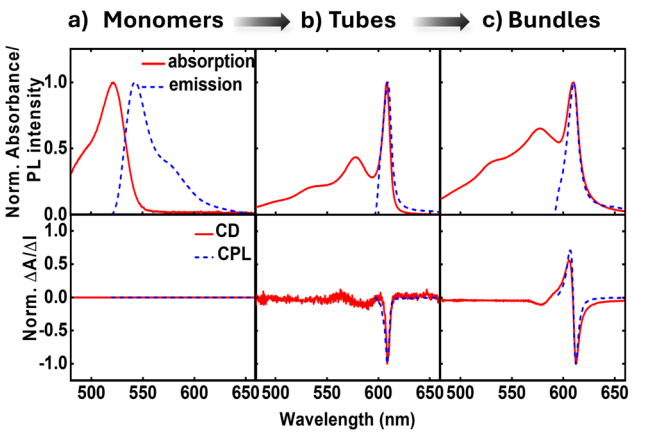

Fig. 2 Experimental spectra of C8O3 monomer in ethanol (a), and of tubes (b) and bundles (c) in thin film. Top panels show normalized absorbance and emission spectra; bottom panels show normalized CD and CPL spectra. $\Delta A = A_L - A_R$ and $\Delta I = I_L - I_R$, where A is absorbance, I is emission intensity and the $L(R)$ subscript refers to left(right) circular polarization of incident light.

demonstrate that the main peak at 610 nm is polarized along the tube axis and is therefore termed the "longitudinal mode," while the 575 nm peak is attributed to a "transverse mode" with polarization perpendicular to the tube axis.[41,50,51]

Tubes and bundles have similar absorption and emission spectra, but qualitatively different chiroptical responses. Tubes exhibit monosignate CD and CPL spectra, peaking at the same wavelength as the longitudinal absorption peak. A very weak, bisignate signal can be noticed in the region of the transverse absorption band. On the opposite, bundles display an intense doublet both in CD and CPL spectra in the region of the longitudinal absorption maximum.

The monosignate feature observed in CD spectra of tubular aggregates is a notable chiroptical anomaly. Just as the intensity of an absorption peak is quantified by its oscillator strength (proportional to the transition frequency times the squared electric transition dipole moment), the intensity of a CD peak is quantified by the associated rotational strength.[43] For a transition between the ground state $|g\rangle$ and an excited state $|f\rangle$, the rotational strength, R_{gf}, is

$$R_{gf} = \mathrm{Im}\left(\left\langle g\left|\hat{\vec{\mu}}\right|f\right\rangle \cdot \left\langle f\left|\hat{\vec{m}}\right|g\right\rangle\right) \quad (1)$$

where Im takes the imaginary part of the argument, and $\hat{\vec{\mu}}$ and $\hat{\vec{m}}$ are the electric and magnetic dipole moment operators, respectively. A theorem, originally derived by Condon[43] and reported in ESI,† proves that the sum of the rotational strengths for all transitions and hence the integrated area beneath a CD spectrum (plotted against transition energies) must vanish. Supramolecular chirality nicely illustrates this principle. Chiral aggregates usually show CD doublets attributed to an asymmetric arrangement of electric transition dipole moments, which leads to the CD contribution called μ–μ coupling.[43,52,53] The asymmetric arrangement of electric transition dipole moments within a chiral aggregate can be associated with an effective magnetic dipole moment so that the chiroptical effect can be described in terms of the rotational strength of eqn (1).[53,54] For a chiral dimer of interacting molecules, the μ–μ coupling contribution to the rotational strength produces two peaks of opposite sign centered around the monomer absorption frequency, ω_0.[25,43] The intensity of the two peaks approximately goes as $\pm\omega_0\vec{r}_{12}\cdot(\vec{\mu}_1 \times \vec{\mu}_2)$, where $\vec{r}_{12}$ is the vector joining molecules 1 and 2, and $\vec{\mu}_{1/2}$ denotes the electric transition dipole moments of the molecules, confirming the sum rule at least in the limit of weak exciton coupling.§ Even in larger aggregates, μ–μ coupling results in CD doublets which approximately obey the sum rule.[23]

If the relevant transition of the monomer is characterized by a sizeable transition magnetic dipole moment besides the electric dipole moment, additional contributions, due to μ–m coupling, appear that are particularly significant for weakly allowed transitions.[53] The μ–m coupling is dubbed intramolecular or intermolecular when it involves dipoles centered on the same or different molecules, respectively.[53] Intramolecular μ–m coupling implies sizeable electric and magnetic transition dipole moments on the same molecule, sharing a common component, and is only possible in inherently chiral molecules. Intramolecular μ–m coupling offers a possible explanation for the single CD peak in the spectrum of individual tubes.[43,55] CD spectra of inherently chiral molecules are often characterized by a monosignated peak, the sum rule being satisfied by CD peaks located at high energies, outside the conventional spectral window of analysis.[56]

C8O3 molecules can exist in twisted conformations due to the formation of intramolecular hydrogen bond between carboxylic groups,[38] but the absence of optical activity in solution indicates a rapid interconversion between enantiomers. On the other hand, when a twisted C8O3 molecule is stuck within an aggregate, steric constraints may prevent the interconversion, giving rise to a neat chiroptical response, consistent with our recent experimental results.[41] Support to this hypothesis comes from spectra collected from aggregates in thin film upon heating at 388 K to disrupt the supramolecular organization. In these conditions, the absorption spectrum closely resembles the monomer spectrum in ethanol (Fig. 2 and 3), supporting the disaggregation of the tube, but a faint monosignated CD peak emerges near the monomer absorption region (Fig. 3), suggesting that chiral monomers are freed upon the disassembly of bundles and tubes, allowing for the acquisition of their chiroptical response prior to racemization. The absorption and CD spectra of Fig. 3 closely resemble those reported in Fig. 3(B) and (G) of ref. 41, acquired in the early stages of C8O3 aggregation.

While the CD signal of Fig. 3 could be due to the presence of small clusters of poorly interacting chiral C8O3 molecules, we point out that the racemization process of isolated C8O3 molecules can be slower in the film than in ethanol solution, since ethanol competes with the formation of intramolecular hydrogen bonds,[57,58] speeding up the interconversion between enantiomers. In any case, the monosignate CD spectrum of

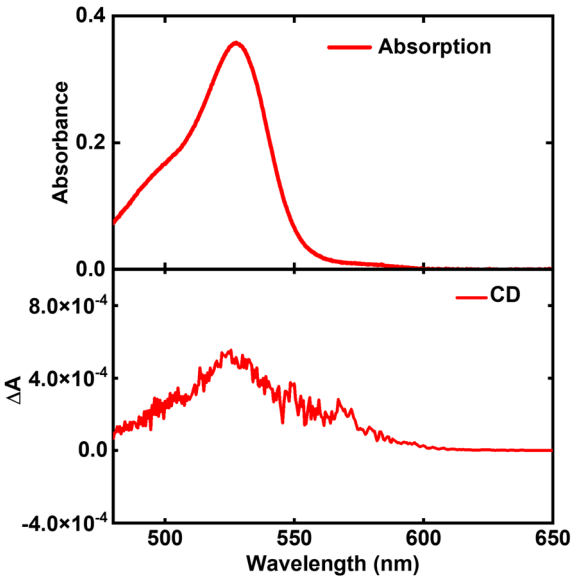

Fig. 3 Absorption (upper panel) and CD spectrum (lower panel) of C8O3 aggregates in thin film, after they have been heated progressively to 388 K until the aggregates are disassembled.

Fig. 3 can only derive from the intrinsic chirality of C8O3 molecules.

As demonstrated by the statistical analysis in ref. 42, the sign of CD spectra for C8O3 aggregates can differ among different samples and even in different zones of the same sample. This suggests that the chirality of monomers, released upon disrupting the aggregates, also varies within the sample, depending on the chirality of the original aggregates.

2.2 C8O3 monomer: the model

C8O3 (Fig. 2a) is an amphiphilic cyanine dye with a positively charged Cy3 polymethinic bridge, long alkylic C8 chains linked to one nitrogen of the benzimidazolium rings, and C3 chains ending with carboxylic groups linked to the opposite nitrogen atom (*cf.* Fig. 1). In the crystal structure,[38] two distinct configurations of C8O3 chromophoric cores, planar and twisted, are observed. The side carboxylic groups of C8O3 are prone to form intramolecular and intermolecular hydrogen bonds, affecting the geometry of the chromophoric core. Specifically, molecules forming intermolecular hydrogen bonds show planar cores, while those forming intramolecular hydrogen bonds show a twisted core, with an 18° dihedral angle between the cyanines' benzimidazolium rings (*D* in Fig. 4). While the whole crystal is a racemate, the distorted monomers in the crystal structure of C8O3, exhibit the axial chirality typical of biaryls.[59]

Quantum chemical calculations (Gaussian 16 suite[60]) are exploited to gain information on the monomeric unit. For computational convenience, all calculations are done on the chromophoric core, *i.e.* substituting all pendant chains with methyl groups (*cf.* Fig. 4). The DFT-optimized molecular structure in the gas-phase (B3LYP, 6-31G(d)) leads to a planar, non-chiral structure. TD-DFT calculations, using different functionals (B3LYP, PBE0, CAM-B3LYP and M062X; 6-31G(d) basis set) were run on the optimized (non-chiral) gas phase structure and on the chiral *S*-axial (S_a) enantiomer of the C8O3 core as extracted from crystallographic data (*cf.* Fig. 4).[38] Relevant results are reported in Tables S1 and S2 in ESI.† For both geometries, the four adopted functionals give very similar results, suggesting that the nature of the lowest energy states is properly captured by all functionals. In both structures, all functionals show that the second excited state, S_2, is a dark state located at much higher energy than the lowest excited state, S_1, so that low-energy spectral properties can be safely described just accounting for S_1.[31,61] As expected, the chiral and non-chiral structures have similar oscillator strength and electric and magnetic dipole moments, but the angle between the electric and magnetic transition dipole moments is 90° for the non-chiral structure, leading, as expected, to vanishing rotational strength.

More interesting for our aims are results obtained for the axially chiral structure that, for the lowest energy transition, has sizable and non-orthogonal electric and magnetic transition dipole moments (angle $\alpha = 89.5°$, right lower panel of Fig. 4). This results in a monosignate CD spectrum with sizable rotational strength (*cf.* ESI, Table S1†). Of course, the *R*-axial enantiomer has the opposite rotational strength, with a μ–m angle of 90.5°.

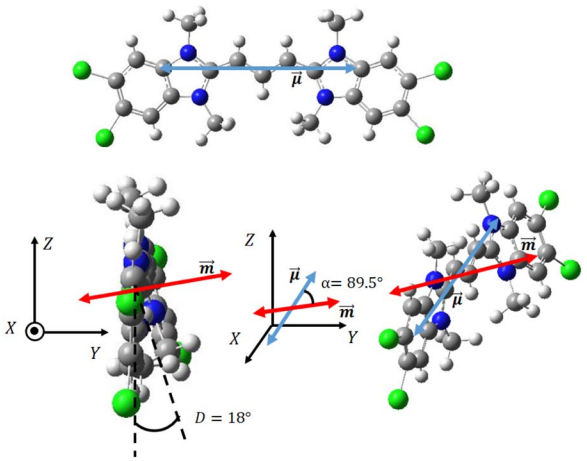

Fig. 4 Upper panel: front view of C8O3 chromophoric core, where the electric transition dipole moment $\vec{\mu}$ is visible as a double headed blue arrow. Left lower panel: side view of twisted C8O3 chromophoric core, where the magnetic transition dipole moment $\vec{m}$ is visible as a double-headed red arrow. Right lower panel: the molecular reference system is rotated to showcase the orientation of both the electric and magnetic transition dipole moments.

In order to build the exciton model for the aggregates, as described in Subsections 2.3 and 2.4, we parametrize the lowest energy transition of the C8O3 dye. Specifically, from the energy and integrated area[62] of the absorption spectrum of Fig. 2 we estimate the monomer transition energy as 2.37 eV and the transition electric dipole moment as 9.6 *D* (molar extinction coefficient from ref. 39, relevant details in Section 3 of ESI).† The magnetic transition dipole moment is estimated from TD-DFT as 1.4 a.u. (that is 2.6×10^{-23} *J*/*T* in SI) with a μ–m angle of 90.5°. With this information, absorption and CD spectra of the twisted chiral monomer are calculated as shown in Fig. 5 (see Section 6 of ESI for details†). Calculated spectra of Fig. 5 are in qualitative agreement with the high-temperature experimental spectra in Fig. 3. The spectra calculated for a planar chromophoric core are shown in Fig. S2† for comparison. While the absorption spectrum does not significantly depend on the chromophore conformation, the CD spectrum vanishes for the planar core.

2.3 The C8O3 single tube

Having parametrized the model for the monomeric unit, we use it as a building block to construct a plausible model for the supramolecular structure of the C8O3 tube. The C8O3 tubes are made of two concentric bilayers, separated by the interpenetrated C8 alkyl chains.[38] The interaction between the cylindric walls was shown to be negligible in similar aggregates,[63] the overall spectrum being the sum of the spectra of each wall. Accordingly, to simulate the spectra, we consider a single cylindric wall, with a diameter $d = 2$ nm, close to the experimental value of the diameter of the inner wall.[40] The "bricklayer" structure proposed in previous works to rationalize

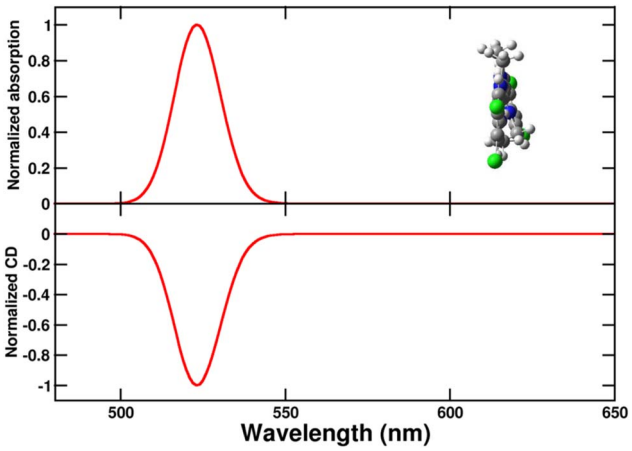

Fig. 5 Normalized absorption (upper panel) and circular dichroism (CD, lower panel) spectra of the twisted chiral C8O3 chromophoric core. A single transition is considered for the monomeric unit (see text), with a Gaussian bandshape and a width $\sigma = 0.045$ eV (*cf.* eqn (S7)).†

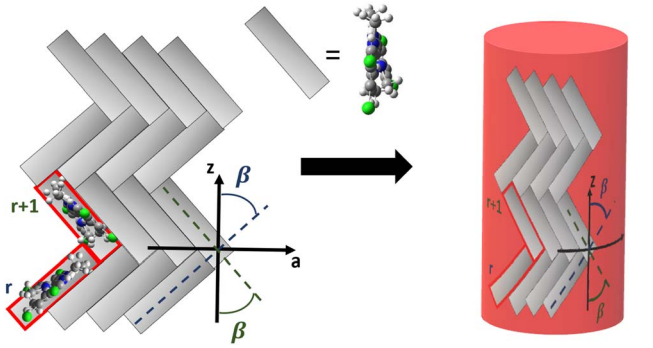

Fig. 6 The herringbone 2D-lattice of C8O3, where cyanines in the r-th row form a β angle with the positive direction of the z axis and cyanines in the r + 1-th row form the same angle with the opposite direction of the z axis (left), is folded to obtain a tube, with z becoming the tube axis (right).

the (chiro)optical properties of C8O3 aggregates[32,64–66] would result in an overall chiral arrangement of the transition electric dipole moments and hence in a strong μ–μ coupling contribution[64] whose characteristic bisignate CD feature is not observed for C8O3 tubular aggregates (*cf.* Fig. 2). Moreover, the bricklayer structure does not account for the presence of absorption bands with different polarization.[63] Quite interestingly, in ref. 63 a herringbone structure was proposed for tubular aggregates of a similar cyanine dye, C8S3, where *two molecules per unit cell* are considered, as needed to account for the presence of absorption bands with different polarization. Here we adopt the same arrangement for the C8O3 chromophores inside the walls, further extending the model to describe the chiroptical properties of the supramolecular assembly.

The tube is constructed from a planar herringbone lattice with two molecules per unit cell (the unit cell is highlighted in red in Fig. 6) that is then folded along the vector $\vec{a}$, to obtain a non-chiral cylinder (see Fig. 6), in close analogy with the arrangement of "zigzag" carbon nanotubes.[67] Within the tube, cyanines are arranged in rows (numbered from bottom to top in Fig. 6). Cyanines in the r-th row are oriented in such a way that their long axis makes an angle β with respect to the tube axis (z), cyanines in the $(r+1)$-th row form the same angle with $-z$. The transition electric dipole moment of each molecule (aligned with the polymethine bridge) is tangent to the cylinder surface. The magnetic transition dipole moments form an angle of 90.5° with the electric dipole moments, hence making the molecules chiral, as discussed in Section 2.2. More details about the geometry are reported in Section 5 of ESI.†

While C8O3 solutions do not show optical activity due to rapid interconversion between enantiomers,[42] steric constraints within the tubes prevent interconversion, keeping the molecules in a fixed conformation and leading to a neat chiroptical response. Moreover, the presence of a distorted C8O3 unit can induce distortions in neighboring monomers, in the so-called *sergeant and soldiers* chirality amplification mechanism.[2] Specifically, a distorted monomer may induce similar distortion in adjacent monomers, without necessarily transferring chirality to the supramolecular level, *i.e.* maintaining a non-chiral supramolecular organization.

To address the optical spectra of the tube, we rely on the exciton model, where only states with a single excited molecule are considered. Specifically, $|n, i\rangle$ represents a state where the i-th molecule in the n-th unit cell is excited. The exciton Hamiltonian accounts for the electrostatic interactions between transition dipole moments:[25,63]

$$H = E_0 \sum_{n,i} |n,i\rangle\langle n,i| + \sum_{n,m,i,j} J(n,i;m,j)|n,i\rangle\langle m,j| \qquad (2)$$

where E_0 is the monomer excitation energy and $J(n,i;m,j)$ is the electrostatic interaction between the electric transition dipole moments of the i-th and j-th molecules in the n-th and m-th unit cells, whose explicit form is given in eqn (S5).† As discussed in ESI (Section 6),† the exciton Hamiltonian can be diagonalized for very large systems (here we consider up to 240 molecules), to obtain relevant eigenstates, as entering the calculation of optical spectra.

The calculated absorption spectrum of the tube (Fig. 7) features two bands, both red-shifted with respect to the monomer. The more intense and red-shifted band ($\lambda_{max} \sim 607$ nm) is longitudinally polarized, while the higher energy band ($\lambda_{max} \sim 560$ nm) has transverse polarization. The presence of two molecules per unit cell allows for two absorption bands with different energies and polarization. In contrast, a "bricklayer" model with one molecule per unit cell would result in all bands sharing the same polarization.[63]

As the overall arrangement of electric transition dipole moments within the herringbone structure is symmetric, the μ–μ coupling contribution to chiroptical spectra vanishes, and the CD spectrum features a single peak in the region of the longitudinal absorption band, in good agreement with experimental data of Fig. 2. Emission and CPL signals occur at the same frequency, in line with Kasha's rule, since both features originate from the lowest excited state observed in absorption and

CD spectra. For these tubular aggregates, the absorption and emission dissymmetry factors are very similar, pointing to negligible geometrical rearrangement upon excitation.[42] The dissymmetry factor calculated for the Kasha's state is estimated as $g_{abs/lum} = 4\frac{R}{D}$, where R and D are the rotational strength and squared electric transition dipole moment, respectively, associated with the transition from the ground state to the Kasha state.[19,68] Our estimate of the dissymmetry factor amounts to $\sim 2 \times 10^{-4}$, much smaller than the experimental value ($\sim 10^{-2}$). This important discrepancy suggests that monomers could have a much more distorted structure inside the tubes than in the crystals.[41] Interestingly, small chiral distortions of the herringbone geometry lead to small μ–μ coupling contributions, and tiny doublets appear in the CD spectrum in the region of the transverse mode (Fig. S4†), in fairly good agreement with experimental observation (Fig. 2).

2.4 The C8O3 bundle

Bundles, which are made out of two or more interwoven weakly interacting tubes,[40,41] represent a further tier in the hierarchical aggregation of C8O3. The simplest model for a bundle accounts for a pair of tubes, each parametrized as described in Section 2.3. The two tubes, at distance l, are arranged with their axes both perpendicular to the vector that joins them and are mutually rotated by an angle Φ, as shown in Fig. 8. The bundle is chiral for $0° < \Phi < 90°$, with the corresponding enantiomeric structures having $-90° < \Phi < 0°$. Calculations were performed for a bundle with inter-tube distance $l = 40$ Å and rotation angle $\Phi = 50°$ (representing a left-handed screw as in Fig. 8). These values were chosen in order to reproduce the energies and relative intensities of the CD and CPL peaks measured experimentally.[42] Calculated absorption, emission, CD, and CPL spectra of the bundle are shown in Fig. 9. In order to account for the thermal population of the first two excited states, emission ($I(\omega)$) and CPL ($\Delta I(\omega)$)spectra are calculated as follows:

$$I(\omega) \propto \omega^3 \sum_k e^{-\frac{E_k - E_1}{k_b T}} \frac{\left|\overrightarrow{\mu_k}\right|^2 e^{-\frac{(\omega-\omega_k)^2}{2\sigma^2}}}{\sigma\sqrt{2\pi}} \quad (3)$$

$$\Delta I(\omega) \propto \omega^3 \sum_k e^{-\frac{E_k - E_1}{k_b T}} \frac{R_k e^{-\frac{(\omega-\omega_k)^2}{2\sigma^2}}}{\sigma\sqrt{2\pi}} \quad (4)$$

where k_b is Boltzmann constant and $T = 300$ K. k runs on the excited states, E_k, $\left|\overrightarrow{\mu_k}\right|^2$ and R_k (see definition in eqn (S11))† are respectively the energy, squared electric transition dipole moment and rotational strength associated to the transition from the ground state to the k-th excited state. Finally, E_1 is the energy of the Kasha state. The dependence of both spectra upon ω^3 is a consequence of the isotropic character of the emission.

While absorption and emission spectra show no significant deviation from those of a single tube (Fig. 7), the CD spectrum of the bundle exhibits two doublets arising from the longitudinal (L) and transverse (T) modes of the tubes, with the longitudinal doublet largely dominating the overall spectrum. The appearance of doublets in the CD spectrum of the bundle is ascribed to μ–μ coupling between the modes of the two interwoven tubes that form a left-handed screw.[9] The μ–μ coupling contribution becomes predominant with respect to the intrinsic chirality present at the molecular level. These features are in very good agreement with the intense CD doublet, centered around the single tube CD peak, observed in the spectrum of the bundle (Fig. 2).

The anomalous observation of a bisignate CPL feature in Fig. 2 deserves some discussion. As already mentioned in ref. 42 a plausible explanation relies on a significant thermal population of an additional state besides the Kasha state, as expected if the energy difference between the two states is comparable to the thermal energy. Upon optical excitation, the system undergoes internal conversion eventually reaching the Kasha state, where it stays long enough to reach thermal equilibrium.[69] If excited states lie close to the Kasha state, their thermal population is responsible for the observation of anomalous (non-Kasha) emission.[70] In the case of the bundle geometry defined above, the calculated interaction between longitudinal modes results in a very small exciton splitting ($\sim$1 meV), smaller than thermal energy at room temperature ($\sim$25

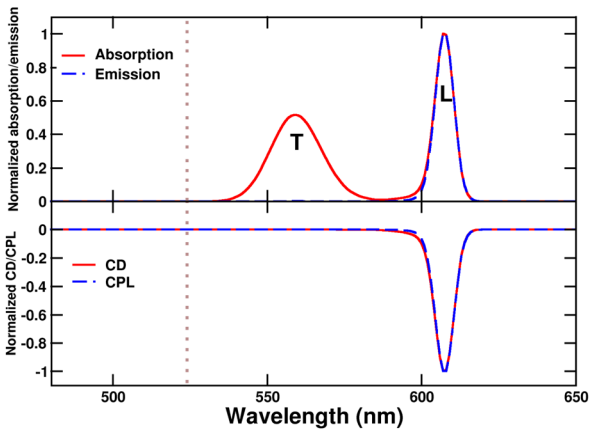

Fig. 7 Spectra calculated for a single C8O3 tube. Upper panel: normalized absorption and emission spectra, L and T stand for "transverse" and "longitudinal" polarization, respectively. Lower panel: calculated CD and CPL spectra. The dotted gray line marks the position of the monomer absorption.

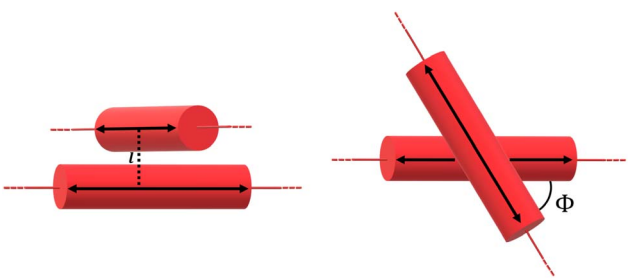

Fig. 8 Side view (left panel) and top view (right panel) of the geometry for the bundle model, where each tube is represented by a red cylinder.

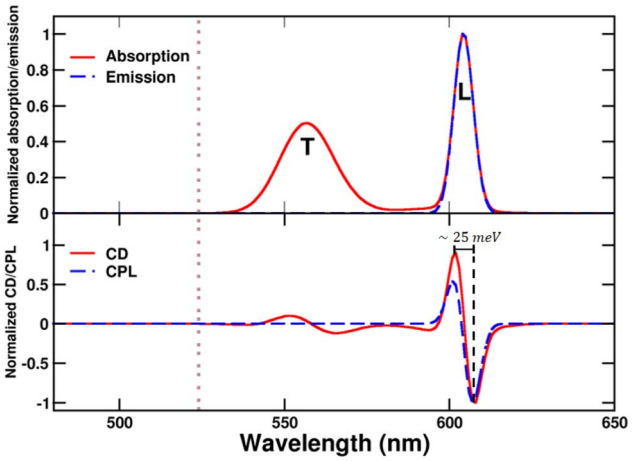

Fig. 9 Spectra calculated for the bundle of C8O3. Upper panel: normalized absorption and emission, *L* and *T* indicate bands that stem respectively from the coupling between longitudinal and transverse modes of the tubes. Lower panel: CD and CPL. Spectra are calculated for a left-handed bundle, with $l = 40$ Å and $\Phi = 50°$. CD and CPL spectra are computed according to eqn (S12)† and (4). Of course, calculations for the corresponding right-handed bundle give CD and CPL spectra of opposite signs. The dotted grey line marks the position of the monomer absorption.

meV). Accordingly, both exciton states are sizably populated, leading to the bisignated CPL observed experimentally.[42] We emphasize that the energy gap between the two exciton states is significantly smaller than the gap estimated from the difference between the energies of the positive and negative peaks in the CPL (or CD) spectra (amounting in this case to ~25 meV). Indeed, when the separation between the two exciton states is tiny, positive and negative signals cancel each other, widening the apparent gap. The calculated dissymmetry factor g_{lum} is approximately 0.08, closely matching the experimental factor.

The μ–μ coupling contribution arising from the interaction between the longitudinal modes of the tubes results in highly intense CD and CPL signals, despite the partial cancellation of peaks due to the low exciton gap. Notably, the rotational strength per monomer in the bundle increases by a 50-fold factor compared to that in the tube, where chirality is solely attributed to the monomer distortion.

3 Conclusions

In this work a bottom-up theoretical approach is presented to elucidate the chiroptical properties of C8O3 aggregates, tracking their evolution across different stages of hierarchical aggregation, from monomers to tubular aggregates, and from tubular aggregates to bundles.

The C8O3 chromophoric core is planar in its equilibrium geometry, but it can be twisted following the formation of intramolecular hydrogen bonds between the side carboxylic groups, inducing axial chirality. While a distinct CD signal is not observed in solution, due to the rapid interconversion between enantiomers, the conformational constraints in the tubular aggregates result in a neat chiroptical response. Within the walls of tubular aggregates, C8O3 dyes adopt a herringbone-like arrangement, leading to the emergence of two distinct absorption bands with orthogonal polarization, namely the longitudinal and transverse modes. The singular CD peak exhibited by C8O3 tubular aggregates directly reflects the intrinsic chirality of the monomers, whereas the herringbone arrangement within the tube is non-chiral, leading to a vanishingly small μ–μ coupling contribution, thus explaining the monosignate CD spectral feature.

The C8O3 bundle is modeled as a chiral dimer of tubular aggregates, wherein the restoration of a CD doublet shape arises from μ–μ coupling interactions between the excitations of constituent tubes. The weak electrostatic interaction between the tubes results in an exciton splitting smaller than thermal energy at room temperature. As a consequence, two excited states can be significantly populated according to a Boltzmann probability distribution, yielding the distinctive anti-Kasha bisignated CPL shown by the bundles. The large CD and CPL signals are attributed to the remarkably large transition dipole moments of the tubes within the bundle, and to the narrow bandwidth that reduces their partial cancellation.

Our analysis explains the origin of the remarkably high g_{lum} value ($\sim 10^{-1}$) measured for the bundles. Indeed, we are able to reproduce it accounting for the electrostatic interaction between tubular aggregates that are organized in a chiral fashion. The tubes themselves are aggregates and, more specifically, J-aggregates and their enormous transition dipole moments explain the amplified dissymmetry factors of the bundles. In other terms, the bundles are aggregates of J-aggregates, which leads to large chiroptical responses. Further enhancement of g_{lum} can be expected for larger electrostatic interactions among the tubes. As an example, Fig. S5† shows how the calculated g_{lum} increases upon decreasing the intertube distance. A shorter distance amplifies the electrostatic interactions between the tubes, which increases the exciton gap and decreases the population of the second excited state. The consequent reduction in mutual cancellation of the CPL peaks leads to a significant increase in the g_{lum} of the first excited state.

The availability of a large set of reliable experimental data on aggregates of C8O3 at various stages of the aggregation process offers a solid basis to develop detailed models for supramolecular chirality, a challenging but extremely rewarding endeavor. Specific information on the aggregate geometry can indeed be extracted from the analysis of experimental spectra and solid structure–property relationships can be extracted at the supramolecular level with the potential to offer reliable guidelines towards the design of novel nanostructured materials with amplified CD and CPL responses.

Data availability

The FORTRAN codes used to calculate the spectra can be found at **https://github.com/francescobertocchi/C8O3_programs**.

Author contributions

F. B. and S. N. equally contributed to the work, with emphasis on theory and experiment, respectively. C. G., T. W. E., M. L. contributed to the experimental part; A. P. and C. S. contributed to the theoretical part. C. G. & A. P: conceptualization. All: methodology, writing and review.

Conflicts of interest

There are no conflicts to declare.

Acknowledgements

This work is part of the Interdisciplinary Thematic Institute QMat of the University of Strasbourg, CNRS, and Inserm. It was supported by the following programs: IdEx Unistra (ANR-10-IDEX-0002), SFRI STRATUS project (ANR-20-SFRI-0012), and USIAS (ANR-10-IDEX-0002-02), under the framework of the French Investments for the Future Program, ERC (project no 788482 MOLUSC). Support from the Indo-French Centre for the Promotion of Advanced Research – CEFIPRA – is also acknowledged (CSRP Proposal No. 6908-2). Work in Parma was supported by PNRR MUR project ECS_00000033_ECOSISTER and benefited from the support of the COMP-HUB and COMP-R Initiative, funded by the Departments of Excellence program of the Italian Ministry for Education, University and Research (MIUR, 2018–2022 and 2023–2027). A. P., C. S. and F. B. acknowledge the support from the HPC (High Performance Computing) facility of the University of Parma, Italy.

Notes and references

§ As discussed in ref. 23, the intensity of the two CD peaks should read $\pm\omega_{\pm}\vec{r}_{12}\cdot(\vec{\mu}_1\times\vec{\mu}_2)$, where $\omega_{\pm}$ defines the frequencies of the two exciton states. In the very weak coupling limit, the exciton splitting is tiny and the two frequencies can be approximated by ω_0, recovering the sum rule. More generally, it can be proved that, if the exciton model is extended to account for doubly excited states, *i.e.* relaxing the Heitler–London approximation, the sum rule is recovered without imposing any approximation on transition frequencies.[23]

1 W. Thomson and B. Kelvin, *Baltimore Lectures on Molecular Dynamics and the Wave Theory of Light*, Cambridge University Press, 1904.
2 M. Green, M. Reidy, R. Johnson, G. Darling, D. O'Leary and G. Willson, *J. Am. Chem. Soc.*, 1989, **111**, 6452–6454.
3 N. Nizar, M. Sujith, K. Swathi, C. Sissa, A. Painelli and K. Thomas, *Chem. Soc. Rev.*, 2021, **50**, 11208–11226.
4 C. Koukoulitsa, A. Karioti, M. Bergonzi, G. Pescitelli, L. Di Bari and H. Skaltsa, *J. Agric. Food Chem.*, 2006, **54**, 5388–5392.
5 N. Berova, L. Di Bari and G. Pescitelli, *Chem. Soc. Rev.*, 2007, **36**, 914–931.
6 W. Zhang, K. Krohn, J. Ding, Z.-H. Miao, X.-H. Zhou, S.-H. Chen, G. Pescitelli, P. Salvadori, T. Kurtán and Y.-W. Guo, *J. Nat. Prod.*, 2008, **71**, 961–966.
7 G. Pescitelli, L. D. Bari and N. Berova, *Chem. Soc. Rev.*, 2011, **40**, 4603.
8 G. Pescitelli, L. D. Bari and N. Berova, *Chem. Soc. Rev.*, 2014, **43**, 5211–5233.
9 N. Berova, K. Nakanishi and R. Woody, *Circular Dichroism: Principles and Applications*, John Wiley & Sons, 2000, pp. 337–395.
10 N. Berova, R. W. Woody, P. Polavarapu and K. Nakanishi, *Comprehensive Chiroptical Spectroscopy: Volume 1-Instrumentation, Methodologies, and Theoretical Simulations*, John Wiley & Sons, 2012.
11 J. P. Riehl and F. S. Richardson, *Chem. Rev.*, 1986, **86**, 1–16.
12 G. Longhi, E. Castiglioni, J. Koshoubu, G. Mazzeo and S. Abbate, *Chirality*, 2016, **28**, 696–707.
13 L. Frédéric, A. Desmarchelier, R. Plais, L. Lavnevich, G. Muller, C. Villafuerte, G. Clavier, E. Quesnel, B. Racine, S. Meunier-Della-Gatta, J.-P. Dognon, P. Thuéry, J. Crassous, L. Favereau and G. Pieters, *Adv. Funct. Mater.*, 2020, **30**, 2004838.
14 K. Dhbaibi, L. Abella, S. Meunier-Della-Gatta, T. Roisnel, N. Vanthuyne, B. Jamoussi, G. Pieters, B. Racine, E. Quesnel, J. Autschbach, J. Crassous and L. Favereau, *Chem. Sci.*, 2021, **12**, 5522–5533.
15 L. Wan, Y. Liu, M. Fuchter and B. Yan, *Nat. Photonics*, 2022, **17**, 1–7.
16 D.-Y. Liu, H.-Y. Li, R.-P. Han, H.-L. Liu and S.-Q. Zang, *Angew. Chem., Int. Ed.*, 2023, **62**, e202307875.
17 J. Crassous, in *Circularly Polarized Luminescence in Helicene and Helicenoid Derivatives*, Springer, 2020, pp. 53–97.
18 P. Rivera-Fuentes, J. L. Alonso-Gómez, A. G. Petrovic, F. Santoro, N. Harada, N. Berova and F. Diederich, *Angew. Chem., Int. Ed.*, 2010, **49**, 2247–2250.
19 J. L. Greenfield, J. Wade, J. R. Brandt, X. Shi, T. J. Penfold and M. J. Fuchter, *Chem. Sci.*, 2021, **12**, 8589–8602.
20 X. Xiao, S. K. Pedersen, D. Aranda, J. Yang, R. A. Wiscons, M. Pittelkow, M. L. Steigerwald, F. Santoro, N. J. Schuster and C. Nuckolls, *J. Am. Chem. Soc.*, 2021, **143**, 983–991.
21 R. V. Person, K. Monde, H.-u. Humpf, N. Berova and K. Nakanishi, *Chirality*, 1995, **7**, 128–135.
22 A. R. A. Palmans and E. W. Meijer, *Angew. Chem., Int. Ed.*, 2007, **46**, 8948–8968.
23 K. Swathi, C. Sissa, A. Painelli and K. Thomas, *Chem. Commun.*, 2020, **56**, 8281–8284.
24 S. Huang, H. Yu and Q. Li, *Adv. Sci.*, 2021, **8**, 2002132.
25 F. Bertocchi, C. Sissa and A. Painelli, *Chirality*, 2023, **35**, 681–691.
26 R. Rodríguez, C. Naranjo, A. Kumar, K. Dhbaibi, P. Matozzo, F. Camerel, N. Vanthuyne, R. Gómez, R. Naaman, L. Sánchez and J. Crassous, *Chem.–Eur. J.*, 2023, **29**, e202302254.
27 Y. Kawabe and S. Kato, *Dyes Pigm.*, 2012, **95**, 614–618.
28 J. Bricks, Y. Slominsky, I. Panas and A. Demchenko, *Methods Appl. Fluoresc.*, 2018, **6**, 012001.
29 X. Guo, D. Yang, R. Sun, Q. Li, H. Du, Y. Tang and H. Sun, *Dyes Pigm.*, 2021, **192**, 109429.
30 A. Delledonne, J. Morla-Folch, M. Anzola, F. Bertocchi, G. Vargas-Nadal, M. Köber, C. Sissa, N. Ventosa and A. Painelli, *J. Mater. Chem. C*, 2021, **9**, 10952–10964.

31 F. Bertocchi, A. Delledonne, G. Vargas-Nadal, F. Terenziani, A. Painelli and C. Sissa, *J. Phys. Chem. C*, 2023, **127**, 10185–10196.
32 C. Didraga, A. Pugžlys, P. R. Hania, H. von Berlepsch, K. Duppen and J. Knoester, *J. Phys. Chem. B*, 2004, **108**, 14976–14985.
33 J. L. Lyon, D. M. Eisele, S. Kirstein, J. P. Rabe, D. A. Vanden Bout and K. J. Stevenson, *J. Phys. Chem. C*, 2008, **112**, 1260–1268.
34 A. Bondarenko, T. Jansen and J. Knoester, *J. Chem. Phys.*, 2020, **152**, 194302.
35 S. Doria, M. Di Donato, R. Borrelli, M. F. Gelin, J. Caram, M. Pagliai, P. Foggi and A. Lapini, *J. Mater. Chem. C*, 2022, **10**, 7216–7226.
36 U. De Rossi, S. Dähne, S. C. J. Meskers and H. P. J. M. Dekkers, *Angew. Chem., Int. Ed.*, 1996, **35**, 760–763.
37 R. Lakes, *Nature*, 1993, **361**, 511–515.
38 S. Kirstein, H. von Berlepsch, C. Böttcher, C. Burger, A. Ouart, G. Reck and S. Dähne, *ChemPhysChem*, 2000, **1**, 146–150.
39 H. von Berlepsch, C. Böttcher, A. Ouart, C. Burger, S. Dähne and S. Kirstein, *J. Chem. Phys. B*, 2000, **104**, 5255–5262.
40 C. Spitz, S. Dähne, A. Ouart and H.-W. Abraham, *J. Chem. Phys. B*, 2000, **104**, 8664–8669.
41 A. Thomas, T. Chervy, S. Azzini, M. Li, J. George, C. Genet and T. W. Ebbesen, *J. Chem. Phys. C*, 2018, **122**, 14205–14212.
42 M. Li, S. Nizar, S. Saha, A. Thomas, S. Azzini, T. W. Ebbesen and C. Genet, *Angew. Chem., Int. Ed.*, 2023, **62**, e202212724.
43 E. U. Condon, *Rev. Mod. Phys.*, 1937, **9**, 432–457.
44 M. Kasha, *Radiat. Res.*, 1964, **3**, 317–331.
45 F. Terenziani and A. Painelli, *Phys. Rev. B: Condens. Matter Mater. Phys.*, 2003, **68**, 165405.
46 M. Anzola and A. Painelli, *Phys. Chem. Chem. Phys.*, 2021, **23**, 8282–8291.
47 O. Arteaga and R. Ossikovski, *J. Opt. Soc. Am. A*, 2019, **36**, 416.
48 E. Jelley, *Nature*, 1937, **139**, 631.
49 F. Spano, *Acc. Chem. Res.*, 2009, **43**, 429–439.
50 A. Pugžlys, P. R. Hania, R. Augulis, K. Duppen and P. H. M. van Loosdrecht, *Int. J. Photoenergy*, 2006, **2006**, 14976–14985.
51 H. von Berlepsch, S. Kirstein, R. Hania, A. Pugžlys and C. Böttcher, *J. Phys. Chem. B*, 2007, **111**, 1701–1711.
52 J. G. Kirkwood, *J. Chem. Phys.*, 1937, **5**, 479–491.
53 T. Bruhn, G. Pescitelli, S. Jurinovich, A. Schaumlöffel, F. Witterauf, J. Ahrens, M. Bröring and G. Bringmann, *Angew. Chem., Int. Ed.*, 2014, **53**, 14592–14595.
54 D. P. Craig and T. Thirunamachandran, *Molecular Quantum Electrodynamics*, Academic Press, 1984.
55 C.-F. Chen and Y. Shen, *Introduction to Helicene Chemistry*, Springer, 2017.
56 S. M. Somasundaran, S. V. K. Kompella, N. Mohan, S. Das, A. Abdul Vahid, V. Vijayan, S. Balasubramanian and K. G. Thomas, *ACS Nano*, 2023, **17**, 11054–11069.
57 A. J. A. Aquino, D. Tunega, G. Haberhauer, M. H. Gerzabek and H. Lischka, *J. Phys. Chem. A*, 2002, **106**, 1862–1871.
58 F. Bertocchi, D. Marchetti, S. Doria, M. di Donato, C. Sissa, M. Gemmi, E. Dalcanale, R. Pinalli and A. Lapini, *Chem.–Eur. J.*, 2024, **30**, e202302619.
59 E. Eliel, S. H. Wilen and L. N. Mander, *Stereochemistry of organic compounds*, John Wiley & Sons, 1994.
60 M. J. Frisch, G. W. Trucks, H. B. Schlegel, G. E. Scuseria, M. A. Robb, J. R. Cheeseman, G. Scalmani, V. Barone, G. A. Petersson, H. Nakatsuji, X. Li, M. Caricato, A. V. Marenich, J. Bloino, B. G. Janesko, R. Gomperts, B. Mennucci, H. P. Hratchian, J. V. Ortiz, A. F. Izmaylov, J. L. Sonnenberg, D. Williams-Young, F. Ding, F. Lipparini, F. Egidi, J. Goings, B. Peng, A. Petrone, T. Henderson, D. Ranasinghe, V. G. Zakrzewski, J. Gao, N. Rega, G. Zheng, W. Liang, M. Hada, M. Ehara, K. Toyota, R. Fukuda, J. Hasegawa, M. Ishida, T. Nakajima, Y. Honda, O. Kitao, H. Nakai, T. Vreven, K. Throssell, J. A. Montgomery Jr, J. E. Peralta, F. Ogliaro, M. J. Bearpark, J. J. Heyd, E. N. Brothers, K. N. Kudin, V. N. Staroverov, T. A. Keith, R. Kobayashi, J. Normand, K. Raghavachari, A. P. Rendell, J. C. Burant, S. S. Iyengar, J. Tomasi, M. Cossi, J. M. Millam, M. Klene, C. Adamo, R. Cammi, J. W. Ochterski, R. L. Martin, K. Morokuma, O. Farkas, J. B. Foresman and D. J. Fox, *Gaussian-16 Revision C.01*, Gaussian Inc., Wallingford CT, 2016.
61 F. Terenziani, A. Painelli, C. Katan, M. Charlot and M. Blanchard-Desce, *J. Am. Chem. Soc.*, 2006, **128**, 15742–15755.
62 J. Lakowicz, *Principles of Fluorescence Spectroscopy*, Springer, 2006, vol. 1.
63 D. Eisele, C. Cone, E. Bloemsma, S. Vlaming, C. Kwaak, R. Silbey, M. Bawendi, J. Knoester, J. Rabe and D. Vanden Bout, *Nat. Chem.*, 2012, **4**, 655–662.
64 C. Spitz, J. Knoester, A. Ouart and S. Daehne, *Chem. Phys.*, 2002, **275**, 271–284.
65 C. Didraga, J. A. Klugkist and J. Knoester, *J. Phys. Chem. B*, 2002, **106**, 11474–11486.
66 C. Didraga and J. Knoester, *J. Lumin.*, 2004, **110**, 239–245.
67 A. Jagadeesan, T. Krithiga and V. Dhananjeyan, *Carbon Nanotubes: Synthesis, Properties and Applications*, IntechOpen, 2020.
68 L. Arrico, L. Di Bari and F. Zinna, *Chem–Eur. J.*, 2021, **27**, 2920–2934.
69 D. Giavazzi, F. Di Maiolo and A. Painelli, *Phys. Chem. Chem. Phys.*, 2022, **24**, 5555–5563.
70 K. Veys and D. Escudero, *Acc. Chem. Res.*, 2022, **55**, 2698–2707.